Chapter 2
LITERATURE REVIEW

2.1 Prologue

This chapter starts with a discussion on the primary components of asphalt mastics. The details about fillers, binders, filler-binder ratio, and the interaction between filler and binder are explained further. The second section covers the rheological testing details of the asphalt binders as well as the asphalt mastics. The fundamentals of rheology, the working of DSR, and the background calculations behind the obtained results are thoroughly explained. The third section highlights the fatigue cracking in asphalt pavements, the mechanism of cracking, and the mode of loading. In addition, different types of fatigue tests on mixes and binders/mastics are detailed, along with their advantages and disadvantages. The same section also briefly describes different testing geometries typically used in the DSR for the rheological testing of asphalt samples. The final section focuses on the problem statement's description and the research gaps identified from the literature review.

The term ‘asphalt binder’ and ‘bitumen’ is used interchangeably throughout the whole thesis for the binder, whereas the mixtures are represented by adding the term ‘mixture’ such as ‘asphalt mixture’ and ‘bituminous mixture.’ In addition, the relative proportion of filler with respect to the binder in mastics or the mixes are notified interchangeably by different terminologies in the thesis, such as filler content, filler dosage, filler-binder ratio, and filler volume concentration (for the proportion on a volume basis).

2.2 Asphalt mastic

The combination of mineral filler and asphalt binder, i.e., mastics, is considered a fundamental dispersed system in an asphalt mixture [50]. The behavior of the asphalt mastics is dependent

on the constituents and their relative proportion. Therefore, the systematic examination of these factors aids in a proper mix design, resulting in a better performing asphalt mixture. In view of this, the current section explores the components of asphalt mastics that govern its fatigue behavior.

2.2.1 Mineral filler

The finest component of the aggregates in an asphalt mixture having a particle size less than 0.075 mm (India, United States) or 0.063 mm (Europe) are termed mineral fillers [10]. However, MoRTH-2013 stated that the mineral filler passes 100% through 0.6 mm sieve, 95-100% through 0.3 mm sieve, and 85-100% through 0.075 mm sieve. They can be classified as natural filler and waste filler based on their source of inheritance. Natural fillers, such as limestone, granite, basalt, etc., are directly mined from the earth's crust and hauled to the required locations, whereas the waste fillers are generated from industrial, agricultural, and construction sectors and are discarded. Some examples of waste fillers found in recent literature include Cement kiln dust [51] borogypsum [52], recycled brick powder [53,54], phosphorus[55], fly ash [56,57], phosphate waste [58], coal waste powder [59], waste ceramic materials[60], rice husk ash [61], taconite [62], waste bleaching clay [63], baghouse fines [64], marble waste dust [65], granite waste dust [66], steel wool or steel fiber [67], sewage sludge ash [68], municipal solid waste incineration ash [69], zirconium tungstate [70], ceramic waste [71], magnetite [72], steel slags and blast furnace slags [73], glass powder [74], recycled waste lime [75], and Jordanian oil shale fly ash [76] have been proved as the performance enhancer when investigated as filler.

The Indian codal provisions (MoRTH guidelines) have specified only two parameters, namely plasticity index, and gradation, to characterize fillers. The Superpave guidelines have also provided only a range of filler-binder ratios (0.6-1.2 by weight) for the satisfactory performance

of a mix. Hence, the standard specifications are insufficient to accurately characterize the properties of the fillers. The fillers have a vast range of physical properties which contributes to the behavior of fillers in the asphalt mastics as well as mixtures assessed by the set of characterization tests [77] like specific gravity (SG), particle (grain) size distribution, Rigden voids (RV), methylene blue value (MBV) test, X-Ray Diffraction (XRD), Brunauer, Emmett, and Teller (BET) test, etc. Hence, the filler-binder ratio range should be redefined based on the more fundamental methodology rather than using empirical values.

Environmental pollution from the wastes produced by industries is a serious global issue and a threat to sustainability. Industrial wastes not only cause human health hazards but are also responsible for the imbalance in the ecosystem, groundwater contamination, and vegetation degradation [78]. Dimension stone sector is also a major waste generating source where the cutting and processing activities contributes approximately 10 million tons annually [79]. The dimension stone is one of the most used construction materials in buildings, monuments, temples, and hotels, especially in cladding, flooring, and paving [80]. India is the third largest producer of dimensional stone in the world [79]. Marble and Limestone are the most popular dimension stones used in different sectors across the globe. Moreover, the excavation activities at the quarry for the procurement of sand, gravel, construction aggregate, etc., generate a huge quantity of dust, a waste material which is generally non-hazardous and inert in nature but can cause serious health issues especially the respiratory problems. Therefore, the sustainable solution to the waste disposal is very challenging and the employment of these wastes in the pavement can be an efficient solution to the aforementioned problems.

2.2.2 Asphalt Binder

Bitumen or asphalt binder can be defined as the class of natural or manufactured cementitious substances which are black or dark black with the primary composition of high molecular

weight hydrocarbons [81]. It is obtained from the fractional distillation of crude oil [82] and consists of organic molecules having varying compositions ranging from highly polar and condensed aromatic rings to non-polar saturated hydrocarbons [83]. In addition to the predominant hydrocarbons, other compounds containing Nitrogen, Sulfur, Oxygen, and traces of metals like Calcium, Magnesium, Iron, Nickel, and Vanadium also exist in the bitumen system [84]. The exact composition of the bitumen constituents varies, depending on many factors such as the quality of crude oil, the type of bitumen manufacturing process, and the modification [85]. [77]Bitumen is a complex hydrocarbon in which the arrangement of Carbon and Hydrogen atoms is in a branched, cyclic, or aromatic manner which is responsible for the intrinsic mechanical properties of the binder [86]. It is divided into four generic groups: Saturates, Aromatics, Resins, and Asphaltenes, popularly known as SARA fractions. The first three groups are collectively called maltenes and are regarded as the oily matrix [87]. The asphalt binder can be considered a colloidal structure in which insoluble asphaltenes are dispersed in the maltenes phase [88]. The asphaltenes, the polar aromatic molecules, are the principal viscosity enhancing components in bitumen owing to their high molecular weights [85]. Therefore, the stiffness of the binder is primarily dependent on asphaltenes. The proportion of asphaltenes varies from 5-25% inside the bitumen [89]. Resins are also polar and are acclaimed as dispersing agents or peptiser for asphaltenes [90] . The relative proportion of resins and asphaltenes dictates the behavior of bitumen as solution (SOL) type or gelatinous (GEL) type [91]. The majority of bitumen are aromatics, non-polar viscous oils, i.e., about 40-65%. They are the dispersion medium for asphaltenes and have a high dissolving ability [92]. The non-polar viscous oils having a white or straw color which forms about 5-20% of bitumen, are known as saturates, including waxy and non-waxy types. The amount of asphaltenes and saturates with respect to resins and aromatics is known as the colloidal index (CI) or Gaestal Index. High CI represents GEL type, whereas low CI indicates SOL type bitumen [93]. The

maltene phase has a high amount of secondary bonding, due to which the asphalt binder is temperature sensitive. The bonding breaks with high temperature, and hence stiffness/viscosity decreases. The bitumen can be separated into various fractions using different techniques such as chromatography, filtration, molecular distillation, solvent extraction, etc. [89].

The Superior Performance Asphalt Pavements (SUPERPAVE) is the result of the asphalt research taken under the SHRP established in 1987 with the motive of developing a new mixture and binder specifications that can provide the most accurate testing results and simulates actual pavement conditions. The PG system bifurcates the bituminous binder based on two temperature limits within which the binder performs satisfactorily. The two temperature limits correspond to the response of binders at high exposure temperatures and low service temperatures, respectively [94]. The SHRP's asphalt research program focused on various pavement areas: low temperature thermal cracking, intermediate temperature fatigue, high temperature rutting, adhesion, aging, and moisture damage [95–97].

The asphalt binder is commonly used in asphalt mixtures to bind the aggregates and fillers together under the application of loads. It shows a very complex behavior due to its viscoelastic nature, i.e., it behaves like an elastic solid at low temperatures and high frequency, whereas it behaves like a viscous liquid at high temperatures and low frequency. The binder significantly affects the performance of HMA and plays an important role in the durability of pavement in the form of resistance towards fatigue, rutting, and low temperature cracking [82,98–104]. In addition, the fatigue behavior of the asphalt mastics is also a major function of the type of binder used in the preparation of mastics [105,106]. The fatigue crack initiates from the asphalt binder, which is the weakest part of the asphalt mastic [107]. Therefore, investigating the role of asphalt binders in the fatigue characteristics of asphalt mastics will help understand the fatigue cracking in asphalt mixtures and, eventually, the asphalt pavements [108].

2.2.3 Filler-Binder (F-B) ratio

The proportion of filler with respect to the quantity of binder in the asphalt mastic or the asphalt mixture in terms of weight or volume is known as the F-B ratio. The reinforcing effect of fillers within the asphalt matrix varies depending on the type of filler and binder. This can be divided into three broad mechanisms: volume filling, physicochemical interaction, and filler particle interaction effects [109,110]. Volume filling refers to the stiffness of asphalt binder, mainly observed at the lower filler volume fractions. On increasing the filler volume, the filler-binder interfacial effect becomes dominant, which on further increment in filler volume, i.e., higher than a critical value (generally > 40%) diminishes, and the particle interaction effect comes into existence [111]. In other words, volume filling, physicochemical interaction, and filler particle interaction are the dominant improvement mechanism at low, medium, and high filler volume concentrations, respectively [112].

The increase in the F-B ratio causes higher stiffening in asphalt mastics which directly influences the high temperature permanent deformation, fatigue cracking at the intermediate temperature range, low temperature durability, and moisture stability [113–115]. As one of the primary influencing factors affecting mastic performance, selecting the suitable F-B ratio is a judicial decision. A very low F-B ratio makes the mastic so soft that it becomes unsuitable for high temperature performance (rutting). On the other hand, excessive stiffness as a result of high filler content causes the mastic to be brittle, resulting in a lower performance at intermediate (fatigue) and low temperatures (thermal cracking). In an attempt to highlight the importance of optimum stiffening of the binder by the fillers, Harris and Stuart [116] classified the fillers as good and bad fillers. The filler was said to be bad if it made the mixture very stiff, causing problems in lay down or if it did not stiff the mix sufficiently to restrain the binder from draining down [117]. Buttlar et al. [118] incorporated several filler-bitumen ratios and temperatures to study the wide range of asphalt mastics. They postulated that the

physicochemical reinforcement is the dominant mechanism at high F-B ratios, but its role is secondary at low filler contents.

2.3 Rheological Characterization of Asphalt Materials

The study of the internal response of any material to the generated stresses in terms of flow and deformation is known as rheology [92]. It is a derived word from the Greek language where "rheo" translates to flow and "logy" stands for science/study; hence rheology is the study of flow.

2.3.1 Viscoelasticity

As the name suggests, it is the property of a material that exhibits both elastic and viscous behavior depending on the testing conditions, such as temperature and frequency. An ideal elastic material deforms with the application of load and returns to its initial state after the removal of applied loads. The viscous material, on the other hand, undergoes permanent deformation after the load application. The asphalt binder is a viscoelastic material that displays elastic behavior at lower temperatures and higher frequencies, whereas it shows viscous behavior at higher temperatures and lower frequencies. Hence, temperature and frequency are the most important parameters affecting the rheological properties of the binder. This dependency can be well explained by the theory of linear viscoelasticity, which states that there exists a maximum limit of applied loading below which the material's response is dependent on the frequency/loading time and temperature only, irrespective of the magnitude of loading. This limit is known as the LVE limit, which is the value of applied strain corresponding to 95% of the maximum complex modulus determined by conducting an amplitude sweep test at a

frequency of 10 rad/sec, as presented in Figure 2.1.

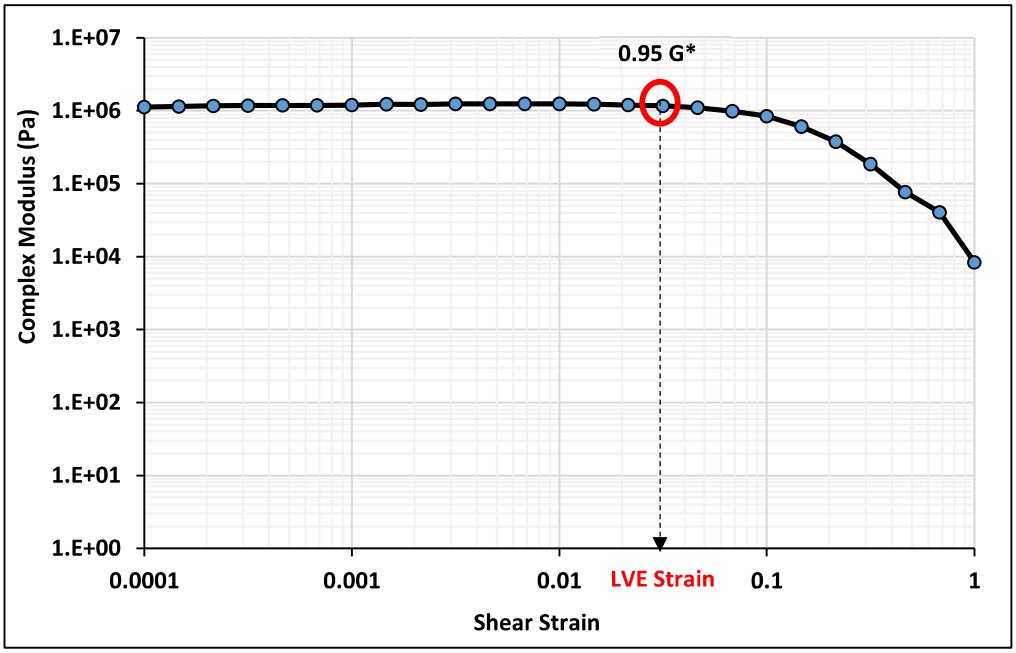

Figure 2.1 LVE limit of asphalt binder/mastic

2.3.2 Aging

The aging of asphalt materials has been an important topic of discussion in recent years, as evidenced by previous researches [31,90,119–125]. It refers to the loss of volatile components and oxidation of the asphalt binder resulting in increased stiffness or brittleness of the materials [126]. In addition to oxidation and loss of volatiles, steric hardening and exudative hardening are the other factors contributing to the aging process. Aging can be irreversible or reversible depending on the type of mechanism. The chemical changes inside the binder due to loss of volatiles, oxidation, and exudation (movement of oily components of the binder to the aggregates) cause irreversible aging. On the other hand, the reorganization of binder molecules for achieving a stable thermodynamic state is attributed to reversible aging in terms of physical hardening. The progressive hardening of asphalt materials as a consequence of aging is a relentless process that may be beneficial from the rutting point of view as it can reduce the

permanent deformation, but it is detrimental from the fatigue aspect as the embrittlement aggravates the cracking susceptibility of the materials [127].

The aging process can be divided into two categories, i.e., short term aging (STA) and long term aging (LTA). Short-term aging occurs during the pavement's construction phase, i.e., mixing, laying, and compaction. The asphalt binder is anticipated to begin to age as soon as it is exposed to hot aggregates and plant burners, continuing through hauling and laying until the final compaction [89]. It is an accelerated process due to exposure of the thin film of asphalt at elevated temperatures. Mixing temperature, type of plant, and silo storage time are the primary factors affecting the STA. Long-term aging, on the other hand, is the result of the progressive oxidation of the asphalt mixture during the pavement's service life [128]. The rate of LTA is slower as a result of in-service exposure to asphalt at relatively lower temperatures [129] and is primarily dependent on the environmental conditions and in-service air void content [130].

The STA and LTA of the asphalt binder can be simulated in the laboratory using the thin film oven test ((TFOT): ASTM D1754)/ rolling thin film oven test ((RTFOT): ASTM D2872) and pressure aging vessel ((PAV): AASHTO R28) respectively as per Superpave binder specifications. There is no separate protocol for aging asphalt mastics; hence, conventional binder aging protocols are also used for mastics aging. Researchers have developed several laboratory testing methods to simulate pavement aging in addition to standardized tests. The STA methods include the shell microfilm test [131], rolling microfilm oven test [132], tilt oven durability test [133], thin film accelerated aging test [134]etc. On the other hand, the Iowa durability test [135], pressure oxidation bomb [136], accelerated aging test device [137], high pressure aging test [138] etc., are some of the LTA laboratory tests.

2.3.3 Dynamic Mechanical Analysis (DMA)

The viscoelastic behavior of asphalt binders can be assessed with the help of Dynamic Mechanical Analysis (DMA) by using a DSR. It can be operated in strain controlled as well as

stress controlled modes. It involves applying the sinusoidal, oscillatory strain and monitoring the resulting stress in strain controlled mode of loading, whereas vice-versa is true for stress controlled testing. The loading is applied to a thin film of bitumen sandwiched between two parallel plates of the DSR, with the lower plate being fixed and the upper plate applying the load. The resulting response is out of the phase with the applied strain/stress, which is attributed to the viscous component of the binder and is related to the dissipation of viscous energy [85]. The elastic material dissipates negligible energy, and hence the phase angle is 0°, whereas the viscous material dissipates all the energy resulting in a 90° phase difference.

Two testing parallel plates are generally used in the DSR, i.e., a plate of 25 mm diameter with a testing gap of 1 mm, and an 8 mm diameter plate with a 2 mm testing gap. The former setup is commonly used at high temperatures, whereas the latter is used at intermediate and low testing temperatures. The shear stress and shear strain are the functions of the radius of parallel plates, due to which their variation is non-uniform from the center to the extremities of the sample. Hence, the corresponding values are calculated at the periphery of the sample by the torque and deflection angle using the following equations:

$$\tau = \frac{2T}{\pi r^3} \tag{2.1}$$

$$\gamma = \frac{r.\theta}{h} \tag{2.2}$$

Where τ is the shear stress (N/mm$^{2)}$), γ is the strain, T is the torque (N.mm), r is the radius of the sample (mm), θ is the deflection angle (radians) and h is the plate gap (mm).

The complex shear modulus (G*) and the phase angle (δ) are the primal viscoelastic parameters obtained from the DSR testing, where G* is the total resistance to deformation on the application of shear loading to the asphalt binder and δ is the time lag or phase lag between the

applied shear stress and strain responses during a test [139]. The variation of shear stress and shear strain is sinusoidal with time; therefore, the complex modulus is calculated as the ratio of absolute stress to strain measured from peak to peak.

$$G^* = \frac{\tau_{max} - \tau_{min}}{\gamma_{max} - \gamma_{min}} \quad (2.3)$$

Where G^* is the complex shear modulus (N/mm^2), τ_{max} and τ_{min} are the maximum, and minimum shear stresses (N/mm^2), γ_{max} and γ_{min} are the maximum and minimum shear strains in a given load cycle.

The complex shear modulus, as the name suggests, is a complex number that can be presented as a combination of storage modulus (real part) and loss modulus (imaginary part):

$$G^* = G' + G'' \quad (2.4)$$

or

$$|G^*| = \sqrt{|G'|^2 + |G''|^2} \quad (2.5)$$

Where $G' = G^*.cos\delta$ is the storage modulus or the elastic component and

$G'' = G^*.sin\delta$ is the loss modulus or the viscous component of the complex modulus

The storage and loss modulus are the stiffness and internal friction indicators, respectively [140]. The ratio of viscous and elastic components of the complex modulus is known as loss tangent and can be expressed as given below:

$$tan\delta = \frac{G''}{G'} \quad (2.6)$$

2.3.4 Time Temperature Superposition Principle (TTSP)

The interrelationship between frequency/loading time and temperature, which allows rheological measurements at multiple temperatures to produce one continuous curve at a wide range of reduced frequencies, is known as TTSP [92]. The materials which follow the TTSP

are known as thermorheologically simple materials. The rheological testing of the asphalt binders by the DSR can only be conducted over a certain range of frequencies, usually three to four decades [89] corresponding to a particular temperature. The obtained data may not completely describe the viscoelastic or rheological behavior of the binders, especially for polymer modified binders. Also, it is not feasible to conduct the test at a wide range of frequencies at each temperature due to very high testing periods. Therefore, the TTSP can be used to shift the data at a reference temperature to obtain the rheological response over a broad range of frequencies.

2.4 Fatigue Cracking

HMA, used as a surface layer in the flexible pavement, is a combination of graded aggregates, mineral fillers, and asphalt binders [141]. These constituents are mixed in a certain proportion to yield a composite strong enough to sustain repeated action of vehicular loading. One of the primary distresses which can reduce the service life of HMA is 'fatigue cracking' [142–144]. The fatigue performance of flexible pavement is the primary function of the cracking resistance of HMA mixtures [145]. Fatigue cracking is caused by the accumulation of cyclic stresses and strains below HMA due to the repeated movement of commercial vehicles [146,147]. Liang et al. [148] define fatigue cracking as a three stage process in which the micro cracks develop in the HMA over time, outgrow into macro cracks, and propagate, leading to the failure of the structure. This phenomenon generally occurs under repeated loading at the intermediate temperature range of 10 ^{o}C to 30 ^{o}C on aged pavements [149,150]. The first fatigue study can be traced back to the investigation of metal, i.e., railroad axles, by Wohler, as stated by Richard [151] who has also been accredited for the development of stress-fatigue life (S-N) curves for fatigue characterization. However, the inclusion of fatigue in the design of asphalt pavements dates back to the early 1940s due to increasing wheel loads and traffic volume [152]. The pavements begin to fail even at small deflections of 0.5-0.8 mm, as reported by Porter [153].

Nijboer and Van der Poel postulated that the cracking in asphalt mixtures is related to the bending stress higher than the flexural strength of the material induced by the moving traffic [154]. Also, Hveem [155] reported the correlation between cracking and repeated deflections with each passing wheel.

A typical fatigue curve is a relationship between the stiffness of the material and the number of cycles, as shown in Figure 2.2 [156]. It can be divided into three phases; phase 1 is called the adaptation phase, in which the rapid decrement in stiffness is observed due to repetitive loading. In addition, microcracks are also developed in this phase under the combined effect of heating, fatigue, and thixotropy. The second phase is known as the quasi-stationary phase, where the rate of stiffness reduction is lower than that of the previous phase. The fatigue damage is dominant compared to other artifact effects, and microcracks show a stable growth rate. Phase III, or the failure phase, is characterized by the development of macrocracks, ultimately leading to failure.

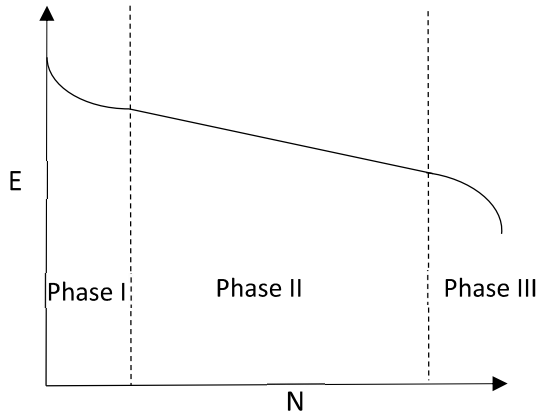

Figure 2.2 Stiffness evolution with the number of cycles [152]

2.4.1 Mechanism of Cracking

The fatigue cracking in asphalt pavements can be broadly categorized into two types: bottom up cracking (BUC) and top down cracking (TDC). The BUC is the most general form of fatigue cracking in which cracks initiate from the bottom of an asphalt layer resulting from high tensile

strains. It is a common cracking mode in thinner asphalt pavements constructed over a granular base or other base layer (MS-2). On the other hand, the TDC originates from the pavement surface under the wheel path and propagates in a downward direction. The TDC appears as the longitudinal cracks in the wheel path, whereas BUC manifests in the form of interconnected cracks [157]. The TDC is generally observed in thick pavements (≥ 160 mm) where the binder aging and tire-pavement interaction generate high localized tensile stresses and result in crack initiation. It is also visible in the asphalt pavements constructed over a rigid base (MS-2). The crack is likely to travel down the pavement up to a depth of 50 mm [158–160].

2.4.2 Mode of Loading

The general fatigue testing of any material, whether the asphalt binder, asphalt mastic, or asphalt mixture, consists of repeated cyclic loading under constant stress (CS) or constant displacement/strain (CD) mode of loading. The CS mode is generally used for thick pavements, whereas the latter mode is used for conventional flexible pavements [161]. In the CS mode of testing, the strain is increased continuously to keep the stress constant. The strain keeps increasing with the ongoing loading, due to which the complete failure of the sample is observed. Hence, the failure point can be precisely defined in the controlled stress mode of testing [162]. On the other hand, in the CD mode of testing, the strain is kept constant by reducing the stress amplitude. After a certain time, this stress magnitude becomes so small that the complete fracture of the sample cannot be observed; therefore, the fatigue failure point is very difficult to obtain in CD mode [162].

2.4.3 Fatigue in Mixes

The fatigue characterization in asphalt mixtures can be done using two main approaches, i.e., the phenomenological approach and the damage/mechanistic/fracture approach. The former approach is most commonly used due to its simplicity, in which the fatigue life of the asphalt

mixture is related to the initial response of the material, such as strain or stress [163]. Initially, the fatigue life prediction was done by the power-law relationship expressed below:

$$N_f = a(\frac{1}{\varepsilon_o})^b \text{ or } N_f = c(\frac{1}{\sigma_o})^d \quad (2.7)$$

Where,

N_f is the number of cycles to failure, σ_o is stress amplitude, ε_o is the applied strain, and a, b, c, and d are the constants that depend on the material and testing conditions [164]. Monismith et al. [165] modified the above equations by including the mixture stiffness (|G*|) to account for the effect of temperature:

$$N_f = a\left(\frac{1}{\varepsilon_o}\right)^b (|G^*|)^c \quad (2.8)$$

The Mechanistic-Empirical Pavement Design Guide (MEPDG) utilized the above model as an input to fatigue prediction, including laboratory to field adjustment factor [166]. The phenomenological approach is very popular owing to its simplicity but lacks in considering the damage accumulation and internal fracture due to fatigue [167].

The fracture mechanics approach accounts for the evolution of damage throughout the pavement's service life and applies to a wider range of loading and environmental conditions. The modeling of asphalt mix using fracture mechanics can be divided into regions, i.e., linear and non-linear. In the linear fracture mechanics, the crack growth in the material was assumed to be in accordance with the Paris law of crack growth. Schapery proposed that the damage in viscoelastic materials can be better represented by a power law [168] which can be expressed as:

$$\frac{da}{dN} = A(\Delta K)^n \quad (2.9)$$

Where,

da/dN is the rate of crack growth with respect to loading cycles

A and n are the fracture properties determined by the experimental testing

ΔK is the stress intensity factor which depends on the testing geometry, mode of fracture, and cracks length. In the non-linear fracture mechanics, the J-integral is used in place of K to express the crack growth rate. The fatigue characterization of asphalt mixtures has been done by several researchers using both linear [169,170] and non-linear fracture mechanics [171,172].

2.4.3.1 Fatigue Testing by Phenomenological Approach

The four point bending beam (4PBB) test is the most popular fatigue test for asphalt mixtures. The fatigue response of asphalt mixtures in the 4PBB fatigue test better simulates the tensile strains in the pavement generated as a result of bending stress induced by vehicular traffic [173]. The induced cracking in the specimen is similar to the bottom-up cracking in asphalt pavements [174].

As the name suggests, the prismatic beam is supported at 4 points (all having free horizontal translation and rotation) and subjected to dynamic loading at two inner bearings or middle thirds of the beam sample, producing uniformly distributed bending moment throughout the mid-span of the beam. The test includes a rectangular beam of 380 mm in length, 63 mm in width, and 50 mm in thickness. The test procedure consists of applying repeated either stress-controlled or strain-controlled cyclic deformation in the form of a sinusoidal waveform (AASHTO T321) or haversine loading (ASTM D7460) which induces the tensile strains at the bottom, similar to what happens in the field [17,175]. The failure point is generally assumed as a 50% reduction in initial stiffness in terms of the number of cycles to failure measured at the center of the beam after the 50^{th} load cycle [129]. The fatigue life of the pavement can be

determined by multiplying a shift factor by the obtained N_f from the 4PBB test [175]. The SHRP postulated that the 4PBB test is superior to other testing methods for evaluating the fatigue properties of asphalt mixtures [176]. Hence, it is the most common and fundamental test for fatigue analysis of asphalt mixtures. The primary laggings in the 4PBB test are complex specimen preparation and longer testing periods. Depending on the selected strain, it can take up to 50 days [177]. Figure 2.3 presents the loading mechanism in a typical 4PBB test.

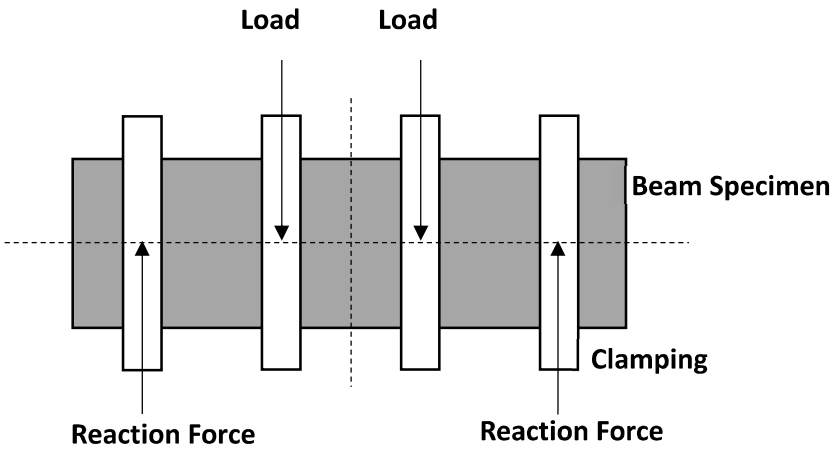

Figure 2.3 Four point bending beam test loading system [145]

The indirect tensile fatigue test (ITFT) is also another test that has been successfully utilized for the fatigue analysis of asphalt mixtures [120,178]. It is conducted on the conventional Marshall compacted specimens 101.6 mm in diameter and 63.5 mm high at intermediate temperatures. The test is conducted in the universal testing machine (UTM) with load application through 13 mm loading strips, as shown in Figure 2.4. The horizontal deformation at the specimen center is measured using extensometers [179] which are then used to calculate the stiffness modulus. The test is conducted in controlled stress mode using a haversine loading waveform at a frequency of 10 Hz.

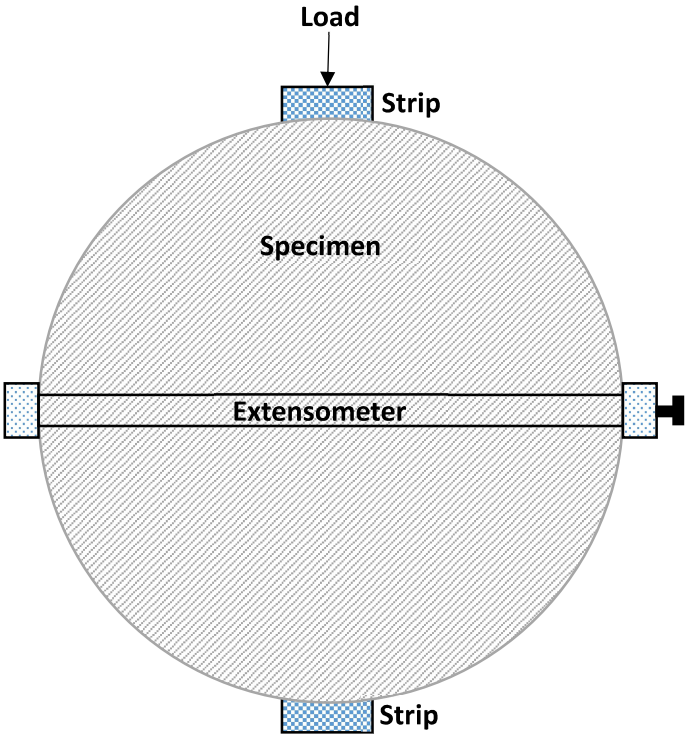

Figure 2.4 Schematic of indirect tensile fatigue test testing arrangement [179]

2.4.3.2 Fatigue Testing by Fracture Mechanics

Fracture mechanics can also characterize the crack initiation and propagation in the materials. It is hypothesized that when the stored energy at the crack vicinity is equal to the required energy for the formation of new cracks, fracture occurs in notched materials [180]. The prerequisite condition is the presence of an existing crack/notch, due to which the majority of fracture tests include a pre-crack or notch. The region near the vicinity of the crack is known as the fracture process zone. The crack growth is negligible if the material in the fracture process zone relaxes because the strain energy is consumed as the surface energy. But the steady rate of crack growth is observed when the strain energy release rate is equal to the fracture toughness resulting in failure. The loading can be characterized as Mode I when the loading direction and initial notch align with the specimen's center line. It solely induces tensile stress at the sample bottom and results in crack propagation [180]. On the other hand, Mixed-

mode loading refers to the setup when loading, notch direction, and center of the specimen are not aligned. The common fracture testing methods are summarized below:

2.4.3.2.1 Single Edge Notched Beam (SEB) Test

The SEB test comprises the three-point bending of the notched asphalt concrete beam, as shown in Figure 2.5. The advantage of the SEB test is that both mode I and mixed-mode loading can be done. The complex sample fabrication and unsuitability for field cores due to the requirement of circular tests are some of the lacunas in the SEB test.

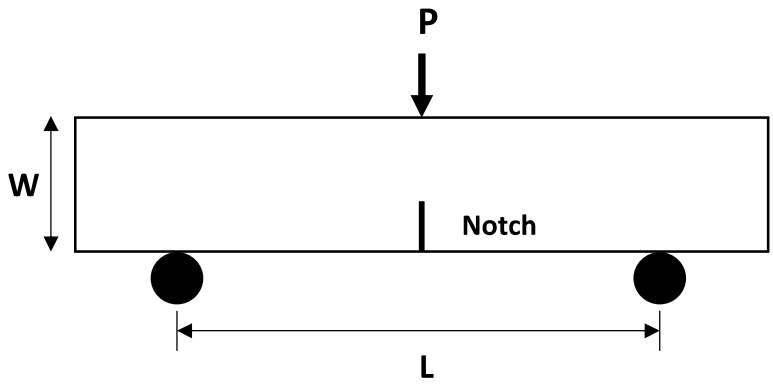

Figure 2.5 Single edge notched beam test [181]

2.4.3.2.2 Disk-Shaped Compact Tension (DCT) Test

The DCT test has been standardized in ASTM E 399 as a standard test method for plane-strain fracture toughness of metallic materials. It differs from SEB as it involves circular geometry having loading holes on each side of the notch, as shown in Figure 2.6. The fracture maximization reduces the geometry-related variability issues, but the stress concentration at holes can lead to premature failure; hence results are erroneous [182]. The sample fabrication is also complicated in the DCT test. Another issue during the testing is the crack deviation from the specimen center.

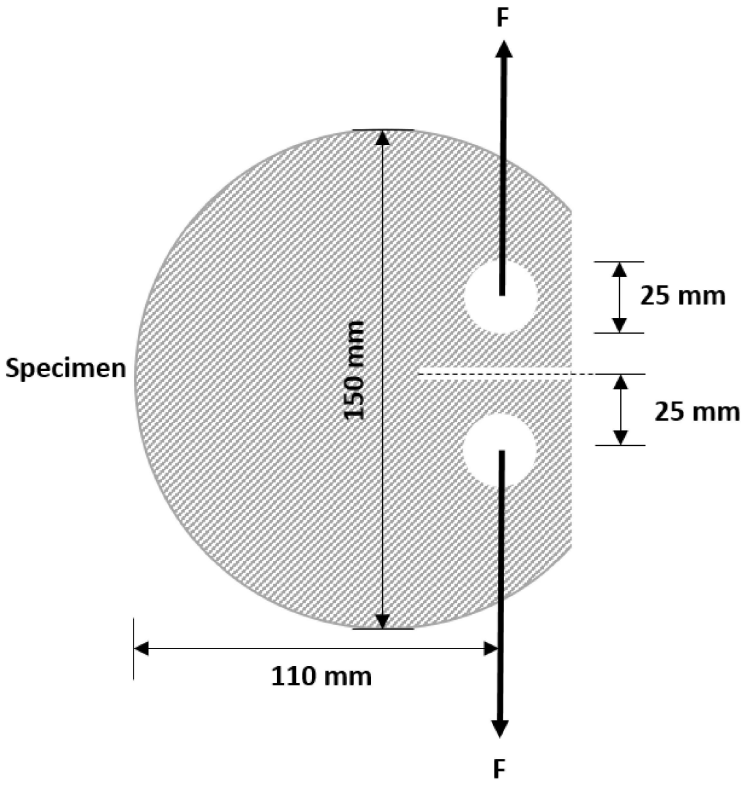

Figure 2.6 Disk shaped compact tension test [183]

2.4.3.2.3 Semi Circular Bending (SCB) Test

The issues related to the SEB and DCT test are solved using the SCB geometry (refer to Figure 2.7). For example, the SCB geometry is simple, easy to fabricate, has high repeatability, and is also suitable for field cores [184–186]. Apart from simplicity, the failure mode of SCB is due to the tensile stress generated due to bending. Chory and Kamuppu proposed the SCB test due to the expense and difficulty of performing the existing test using rock materials [180]. Although it has a lower fracture area as compared to the SEB test, the number of samples becomes twice. It also has great potential for mixed fracture behavior by deviating the inclination angle of the notch or the spacing between supports. It also has three-point loading test arrangement similar to the SEB test.

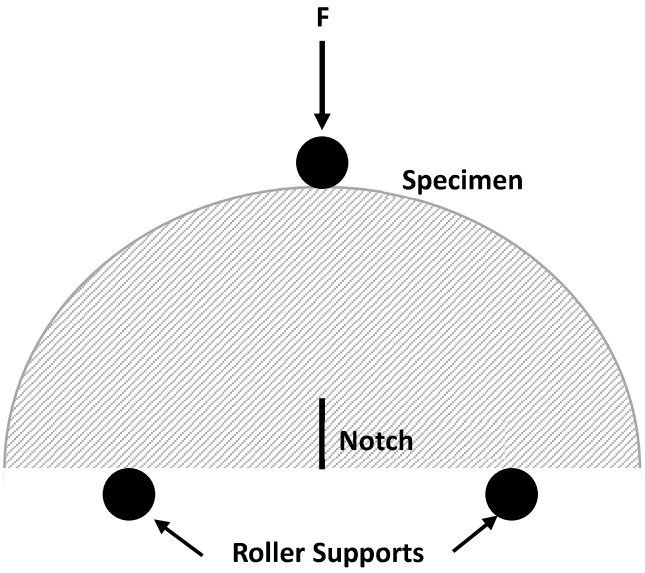

Figure 2.7 Semi circular bending test [187]

2.4.3.2.4 Texas Overlay Test

The rehabilitation of old asphalt and concrete pavements can be done by using an asphalt overlay with a major drawback known as reflective cracking. It is the propagation of underlying cracks on the overlay due to the bending and shearing movements at joints or cracks caused by vehicular loading and environmental factors [188]. The resistance to reflective cracking can be evaluated by an overlay tester developed by Germann and Lytton [189]. It was then modified by the Texas Transportation Institute (TTI) researchers and is now popularly known as the Texas overlay test [190]. The overlay test can also be used to evaluate the fatigue resistance of asphalt mixtures [191]. The Texas standard overlay test setup consists of two aluminium plates; one is stationary, and the other moves back and forth in a horizontal direction with controlled displacements [192] as shown in Figure 2.8. The specimen 150 mm long, 75 mm wide, and 38 mm wide is glued to the top center of the plates, followed by the application of repeated direct tension load. As the loading plate keeps moving, the crack initiates at the specimen bottom and

propagates through the specimen, similar to bottom-up cracking in pavement [192]. The output parameters include loading magnitude, loading time, and plate displacement. The failure point is assumed to be a 93% reduction of the peak load, and the fracture properties are determined in terms of no. of cycles to failure [191].

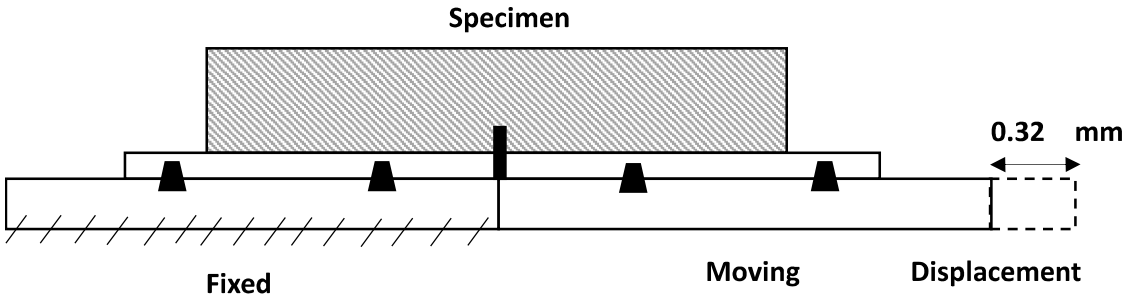

Figure 2.8 Texas overlay test [192]

2.4.3.2.5 Fenix Test

The Fenix test is conducted on semi-circular Marshall or gyratory specimens having 101.6 mm diameter at a loading rate of 1 mm/min [193]. The flat portion of the sample is marked with a notch of 6 mm depth at the center, and two steel plates are fixed on either side of the notch [194] as shown in Figure 2.9. The output parameters in terms of load and displacement are recorded throughout the test to calculate various parameters such as peak load, corresponding displacement, fracture energy, etc. It is based on the uniaxial loading and hence is simple and easy to implement. It also incorporates fracture energy to evaluate the crack resistance and hence skips the complex stress state [195].

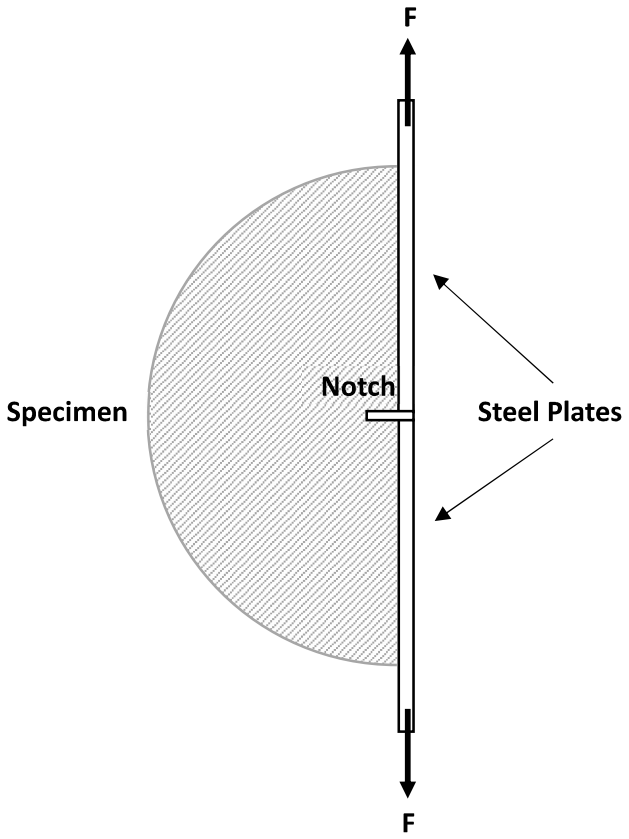

Figure 2.9 Fenix test [194]

2.4.4 Fatigue Testing of Binders or Mastics

Few separate testing protocols or specialized rheological tests have been developed till now, which are dedicated to asphalt mastics. Therefore, asphalt mastics are tested by conducting a similar test or obeying the same protocols as the asphalt binder. The following section presents the common fatigue tests on binders, some of which may or may not be used in the field of asphalt mastics.

2.4.4.1 Superpave Fatigue Parameter

The Superior Performance Asphalt Pavements (SUPERPAVE) specification is the result of the asphalt research taken under the SHRP established in 1987 with the motive of developing a new mixture and binder specifications that can provide the most accurate testing results and simulate actual pavement conditions. It developed the Performance Grading (PG) system for

grading asphalt binder that bifurcates the binder on the basis of two temperature limits within which it performs satisfactorily. The two temperature limits correspond to the response of binders at high exposure temperatures and low service temperatures, respectively [94]. In addition, the SHRP's asphalt research program focused on various areas of pavement, namely low temperature thermal cracking, intermediate temperature fatigue, high temperature rutting, adhesion, aging, and moisture damage [95–97].

The researchers felt the importance of considering fatigue failure as a primary distress during the SHRP, which resulted in the incorporation of fatigue into the SHRP asphalt binder specifications [94,196]. The current Superpave binder specification (AASHTO-MP1-98) states that the resistance of the asphalt binder to fatigue cracking is governed by a stiffness parameter, $|G^*|.\sin\delta$ at a frequency of 10 rad/s and intermediate service temperature, commonly known as fatigue parameter. The binder having the maximum value of $|G^*|.\sin\delta$ not more than 5000 kPa at the average pavement design temperature is believed to be satisfactory in terms of fatigue behavior. This criterion was developed based on limited laboratory testing of mixtures prepared with unmodified binders. The fatigue parameter was able to rank the different binders based on fatigue performance. Also, the upper limit implemented on the binders to perform satisfactorily in terms of fatigue cracking was quite reasonable since the binders tend to age with time resulting in higher stiffness which tends to crack easily [197]. But there are some drawbacks associated with the Superpave fatigue parameter.

Critique: The fatigue parameter is calculated within the LVE region at a very low strain; hence, the higher damage to the pavement during loading cannot be simulated [198]. Moreover, it cannot simulate different traffic conditions due to the testing at a fixed frequency and temperature. In addition, several researchers have reported a poor correlation between the Superpave fatigue parameter and the fatigue life of asphalt mixtures [199,200]. The suitability

of the parameter for the modified binders is also questionable since it was primarily developed for unmodified binders [201].

2.4.4.2 Time Sweep Test

The researchers realized the lacunas associated with the Superpave fatigue parameter, and hence there was an imminent need for a fatigue test method to better characterize the fatigue failure in asphalt binders. As a result, the time sweep (TS) test was developed during National Cooperative Highway Research Program (NCHRP) Project 9-10 [202]. The time sweep test applies the repeated sinusoidal loading to the sample at a predetermined shear strain, frequency, and temperature via DSR. The typical loading scheme in a TS test is shown in Figure 2.10. The time sweep test is considered the most accurate among the existing rheological fatigue test methods since it simulates the actual loading mechanism on the pavement. The pavement degrades with repeated loading and finally results in failure. Similarly, the sample is subjected to repeated loading in the DSR until the failure.

The correlation between the TS results and the asphalt mixture performance was found to be strong in the previous studies hence effectively capturing the contribution of asphalt binder in the performance of asphalt mixtures [202]. The liberty of choosing load amplitude and frequency makes it a better fatigue test than others since one can amend the loading and frequency considering the pavement structure and traffic loading.

Critique: The primary drawback associated with the TS test is the longer testing times. The testing time varies from a few minutes to several days, depending on the type of material and the impractical applied loading. Another major drawback of the TS test is low repeatability. As reported by previous studies, TS's repeatability was very low compared to its counterpart test[203,204]. This is also a serious concern because higher variability in the test results causes uncertainty in determining the actual test results. The situation worsens when determining the

relative ranking between the several binders because the ranking changes while choosing results from different replicates and the results become erroneous. This observation was also reported by previous studies [203,204].

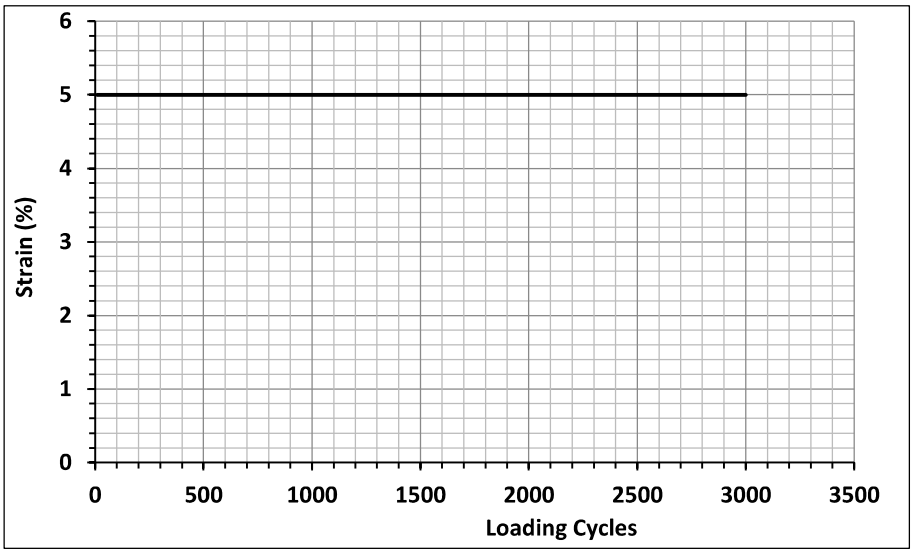

Figure 2.10 Loading scheme in a TS test

2.4.4.3 Linear Amplitude Sweep (LAS) Test

Due to the aforementioned drawbacks in the TS test, despite being the accurate test, an accelerated test was needed, which not only matches the accuracy of the TS test but also be completed in a shorter duration of time and gives good repeatability. Johnson et al. [205] developed an accelerated testing method known as the LAS test to characterize the fatigue behavior of asphalt binders. The LAS test is a two-step procedure, a combination of frequency sweep (FS) test and amplitude sweep (AS) test as per AASHTO TP 101-14. The first step consists of an FS test carried out at a very low strain, i.e., 0.1%, to ensure that the binder is in the LVE region throughout the test. The major output of the test is the undamaged material property of the binder α. It determines the rate of damage evolution in the binder. The parameter α can be calculated in two different ways: either as the reciprocal of slope m of log (|G* |) versus log (frequency) master curve, i.e., 1/m, or can be calculated as 1+1/m. The difference

between the two methods lies in the obtained damage characteristic curve (DCC). This study has evaluated α as 1+1/m because the DCC obtained by this approach is independent of loading history and temperature, which is not the case with α=1/m [206]. The test is conducted at frequencies of 0.2, 0.4, 0.6, 0.8, 1, 2, 4, 6, 8, 10, 20, and 30 Hz, respectively, as per AASHTO TP-101. The later part of the LAS test consists of an amplitude sweep at a fixed frequency of 10 Hz. The applied strain varies from 0.1% to 30% in 300 s or 3000 cycles. This implies that the binder is subjected to accelerated damage way beyond its LVE regime. The applied strain is incremental in nature compared to the constant strain in the TS test, due to which the test is completed within a few minutes, irrespective of the type of material. The typical loading scheme in a LAS test is shown in Figure 2.11. The measured responses from the undamaged and damaged domains are combined and used as inputs to the viscoelastic continuum damage (VECD) analysis framework, the details of which can be found elsewhere [205]. The VECD gives two parameters, A and B, as output which is mathematically formulated to obtain the fatigue life in terms of the number of cycles to failure (N_f) as a function of peak shear strain (γ_o):

$$N_f = A(\gamma_o)^B \tag{2.10}$$

The ability of a material to keep its integrity during loading as a result of accumulated damage is represented by parameter A whereas the B parameter describes the sensitivity of the binder towards the change in strain level. Therefore, a higher A value and a lower value of B are required for a fatigue-resistant material. The relationship in Equation 2.10 is independent of the analysis procedure, and the fundamental difference between various LAS analysis procedures lies in defining A and B. From Equation 2.10, it is clear that the VECD analysis offers the advantage of determining the fatigue life at any strain level from a single test only without actually doing it.

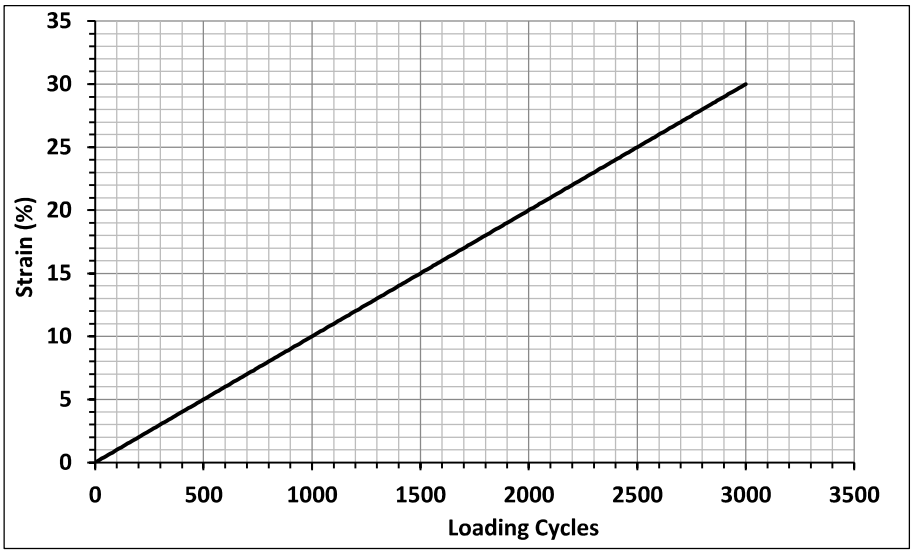

Figure 2.11 Loading scheme in a LAS test

The basic understanding of fatigue cracking as a result of repeated loading is well explored, but the exact point of the fatigue failure is still unknown. There is no definite point that can assure fatigue failure, due to which various scholarly articles have used different criteria to identify the fatigue failure point. Some of the examples include half of the initial complex shear modulus [207], 50% reduction in initial pseudo stiffness [208], peak phase angle [209], Dissipated Energy Ratio (DER) [149], Ratio of Dissipated Energy Change (RDEC) [210,211], maximum stored pseudo strain energy [41], maximum shear stress [212], VECD analysis [181], etc. The VECD is the most commonly used analysis framework, and the standard code, i.e., AASHTO TP-101, is also based on the VECD analysis. A detailed explanation of the two VECD based methods used in this study is described below:

2.4.4.3.1 Dissipated Energy (DE) Based Approach

The Dissipated Energy approach defines the fatigue failure point corresponding to peak shear stress in the material (AASHTO TP-101). The accumulation of damage (D) in the binder, when subjected to repeated loading cycles, can be explained using the following equation [214]:

$$\frac{dD}{dt} = (-\frac{\partial W}{\partial D})^{\alpha} \quad (2.11)$$

W, in the above equation, is the stored potential energy, which can be calculated using equation (3)

$$W = \pi I_D . {\gamma_p}^2 . |G^*| . \sin \delta \quad (2.12)$$

Where γ_p is the maximum strain in a loading cycle, I_D is the initial undamaged dynamic shear modulus in MPa divided by a modulus of 1 MPa [205], $|G^*|$ is the amplitude of the complex modulus, defined as the ratio of maximum stress to maximum strain, while δ is the phase lag between the stress and strain cycle. α in Equation 2.11 is the derived undamaged material property calculated from the slope *m* of log ($|G^*|$) versus log(frequency) master curve [107,206,215–217]. α is equal to 1+1/*m*. There are two methods for calculating the damage evolution rate parameter (α), α=1/*m* or α= 1+1/*m*. The damage characteristic curve (DCC) obtained by using α=1/*m* is dependent on loading history and temperature [206]. On the other hand, α=1+1/*m* makes the DCC independent of temperature and loading history and hence has been used in this study.

Dividing the numerator and denominator on the right hand side of equation (2.11) with *dt,* we get:

$$\left(\frac{dD}{dt}\right)^{1+\frac{1}{\alpha}} = -\frac{\partial W}{dt} \quad (2.13)$$

Now, rearranging the above equation:

$$dD = (-\partial W)^{\frac{\alpha}{1+\alpha}} . (dt)^{\frac{1}{1+\alpha}} \quad (2.14)$$

The damage intensity, *D*, can be calculated by numerically integrating the expression obtained in the form of a Riemann sum. The variation of damage *D* with time can thus be written as:

$$D(t) \cong \sum_{i=1}^{N} \left[\pi I_D {\gamma_p}^2 (|G^*|\sin\delta_{i-1} - |G^*|\sin\delta_i)\right]^{\frac{\alpha}{1+\alpha}} (t_i - t_{i-1})^{\frac{1}{1+\alpha}} \quad (2.15)$$

Further, a mathematical model is fitted between $|G^*|\sin\delta$ and *D(t)* as follows :

$$|G^*|\sin\delta = C_0 - C_1(D)^{C_2} \quad (2.16)$$

C_0, C_1 and C_2 are the model parameters. For normalized values of $|G^*|\sin\delta$, C_0 is equal to 1 [206].

Substituting equation (2.16) in equation (2.12):

$$W = \pi . I_D . {\gamma_p}^2 . (C_0 - C_1(D)^{C_2}) \quad (2.17)$$

Now, differentiating the above equation with respect to *D* yields the following expression:

$$\frac{dW}{dD} = -\pi . I_D . {\gamma_p}^2 . C_1 . C_2 (D)^{C_2 - 1} \quad (2.18)$$

Equating (2.11) and (2.18):

$$\frac{dD}{dt} = (\pi . I_D . {\gamma_p}^2 . C_1 . C_2 (D)^{C_2 - 1})^{\alpha} \quad (2.19)$$

Rearranging the terms and integrating both sides:

$$\frac{D^k}{k} = (\pi . I_D . {\gamma_p}^2 . C_1 . C_2)^{\alpha} . t \quad (2.20)$$

Rearranging the above equation yields the following expression for N_f:

$$N_f = \frac{f\left(D_f\right)^k}{k(\pi I_D C_1 C_2)^\alpha}(\gamma_p)^{-2\alpha} \tag{2.21}$$

In LAS, the value of frequency *f* is 10 Hz. The value of D_f, which is the damage at failure, is calculated using equation (2.15) corresponding to the peak stress value. *k* is equal to 1 + (1-C_2)α.

2.4.4.3.2 Pseudo Strain Energy (PSE) Based Approach

In this method, the evolution of damage in the material, which was previously expressed using equation (2.11), is described in terms of pseudo-strain energy (PSE) as follows:

$$\frac{dD}{dt} = \left(-\frac{\partial W_s^R}{\partial D}\right)^\alpha \tag{2.22}$$

The stored PSE, W_s^R, is the work performed by the binder to resist deformation during a loading cycle. It can be mathematically represented as:

$$W_s^R = \frac{1}{2} \cdot \tau_p \cdot {\gamma_p}^R \tag{2.23}$$

$$W_s^R = \frac{1}{2} \cdot C^*(D) \cdot ({\gamma_p}^R)^2 \,.\,\mathrm{DMR} \tag{2.24}$$

Where the peak pseudo-stiffness $C^*(D)$ can be computed in a given cycle as follows:

$$C^*(D) = \frac{\tau_p}{{\gamma_p}^R \times DMR} \tag{2.25}$$

${\gamma_p}^R$ is the peak pseudo strain, τ_p is the peak stress, and DMR is the dynamic modulus ratio calculated as the ratio of initial $|G^*|$ from strain sweep test and $|G^*|$ from the frequency sweep test. ${\gamma_p}^R$ is calculated from the measured peak strain using the following formula:

$$\gamma_p{}^R = (\gamma_p . |G^*|_{LVE}) \tag{2.26}$$

From equations (2.25) and (2.26), it can be understood that the value of $C^*(D)$ will be equal to 1 within the LVE domain. The increase in strain and accumulation of damage in the binder will reduce its value.

Rearranging equation (2.22) and numerically integrating the resultant similar to equation (2.14), the damage *D* can be calculated as follows:

$$D(t) \cong \sum_{i=1}^{N} \left[\frac{DMR}{2}(\gamma_p{}^R)^2(C^*{}_{i-1} - C^*{}_i)\right]^{\frac{\alpha}{1+\alpha}} (t_i - t_{i-1})^{\frac{1}{1+\alpha}} \tag{2.27}$$

Similarly to the approach in DE based approach, the relationship between the material integrity C^* and damage *D* can be modeled using a mathematical model as shown below [108]:

$$C^* = 1 - K_1(D)^{K_2} \tag{2.28}$$

K_1 and K_2 are model constants obtained by fitting the curve.

Substituting equation (2.28) into equation (2.22) and integrating with respect to *D*:

$$\frac{-\partial W_s^R}{\partial D} = \frac{1}{2}K_1K_2(D)^{k_2-1}(\gamma_p{}^R)^2 \tag{2.29}$$

Equating (2.22) and (2.29), we get,

$$\frac{dD}{dt} = \left(\frac{1}{2}.\left(\gamma_p{}^R\right)^2.K_1K_2\right)^{\alpha}.(D^{K_2-1})^{\alpha} \tag{2.30}$$

Rearranging the terms and integrating both sides yield the following expression:

$$N_f = \frac{f \times 2^{\alpha} \times \left(D_f\right)^J}{J(K_1K_2)^{\alpha}(|G^*|_{LVE})^{2\alpha}}(\gamma_p)^{-2\alpha} \tag{2.31}$$

In the above equation, $J = (1-\alpha K_2+\alpha)$, and D_f is the accumulated damage at failure. The peak of W_S^R versus the number of loading cycles, N, is used to define the failure within the tested specimen. This is illustrated in Figure 2.12(b). The area under total PSE is composed of stores and dissipated strain energies. Figure 2.12 (a) shows the normalized stress-strain relationship obtained for the binder. The area under the solid 45° line shows the total PSE, which is denoted as W_T^R. The dotted curve shows the actual variation of stress up to the peak value. The area under this curve can be approximated using a triangle and represents the stored potential energy, W_S^R. The difference between these two areas is the released dissipated energy which is denoted as W_R^R. W_T^R, W_S^R, and W_S^R can be mathematically defined as follows:

$$W_T^R = \frac{1}{2}(\tau_{undamaged})(\gamma_p{}^R) = \frac{1}{2}(\gamma_p{}^R)^2 \tag{2.32}$$

$$W_S^R = \frac{1}{2}(\tau_p)(\gamma_p{}^R)/DMR = \frac{1}{2}C^*(\gamma_p{}^R)^2 \tag{2.33}$$

$$W_R^R = W_T^R - W_S^R = \frac{1}{2}(1-C^*)(\gamma_p{}^R)^2 \tag{2.34}$$

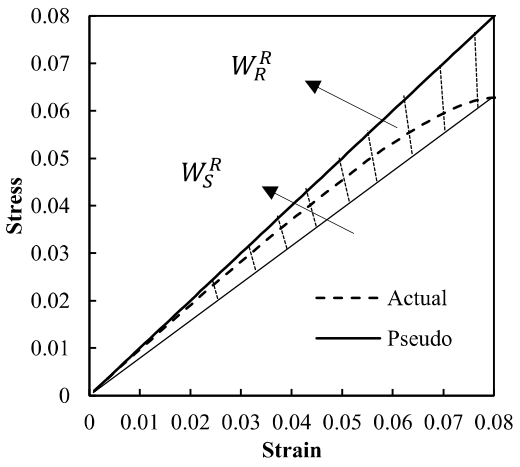

(a)

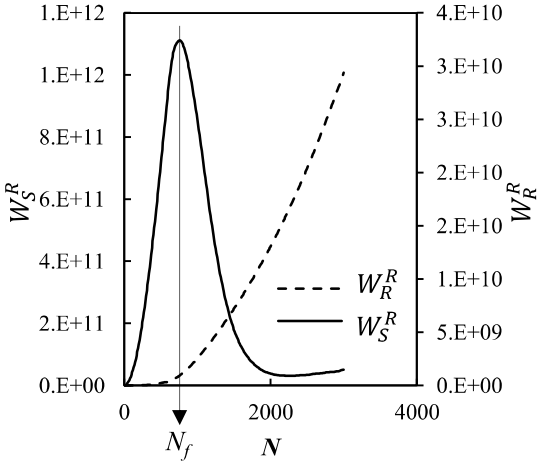

(b)

Figure 2.12 Illustration of PSE approach: (a) Variation of actual and pseudo stress and (b) Identification of failure N_f [217]

2.4.4.4 Binder Yield Energy Test (BYET)

The binder yield energy test (BYET) is another fatigue test conducted at an intermediate temperature to reveal the binder yield characteristics [218]. It is a monotonic test conducted in the rotational mode compared to other fatigue tests conducted in the oscillatory mode. The test consists of applying a monotonic constant shear strain rate of 2.315% s^{-1} to the sample for a time duration of 3600 seconds until the sample achieves a total strain of 4167% as per AASHTO TP-123. The data sampling rate of one data point per two seconds is achieved during the test. The test records both shear stress and strain and is concluded after the yield point known as peak shear stress is reached [219]. The test output includes the computation of the area under the stress-strain curve till the peak shear stress or yield stress, known as yield energy, as shown in Figure 2.13.

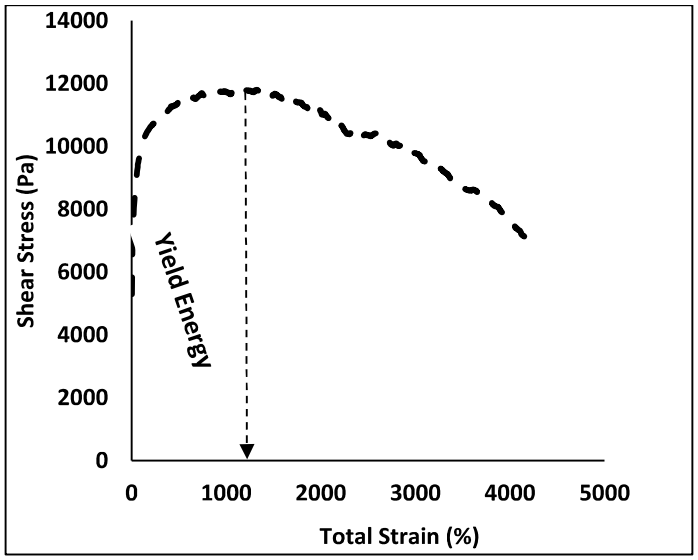

Figure 2.13 Typical output in a binder yield energy test

2.4.4.5 EBADE Test

The EBADE test (an acronym for Ensayo de BArrido de DEformaciones), which means strain sweep (Spanish), was originally developed by Botella et al. [220] to determine the fatigue characteristics of asphalt binders and asphalt mixtures employing the cyclic uniaxial tension-compression test at a frequency of 10 Hz. The test is completed in five different stages, with each stage having a higher constant displacement amplitude than the preceding, with a rest period of 1 min after every stage [221] as shown in Figure 2.14. The binder testing consists of a cylindrical sample 20 mm in diameter and 40 mm high subjected to a wide range of displacements in a single test compared to a constant amplitude in other fatigue tests like TS and Superpave fatigue parameter. The initial 60 μstrain was applied in the first step, followed by successive steps, each having a strain higher than 60 μstrain from the previous step [220].

The asphalt mixture testing involves the application of tension-compression sinusoidal strain to a prismatic specimen in an increasing manner after every 5000 cycles [222]. The test starts with a 25 μstrain in the first stage with a continuous increment of 25 μstrain in each stage [194]. The specimen can be obtained from Marshall, gyratory, or four-point bending beam procedure. The damage is induced in the sample by creating two notches in the center resulting in a reduced area [223]. The typical output variable is the stress from which the complex modulus and dissipated energy are calculated per cycle based on the hysteresis loop [222]. The failure point is defined based on the initial modulus and the failure strain [224].

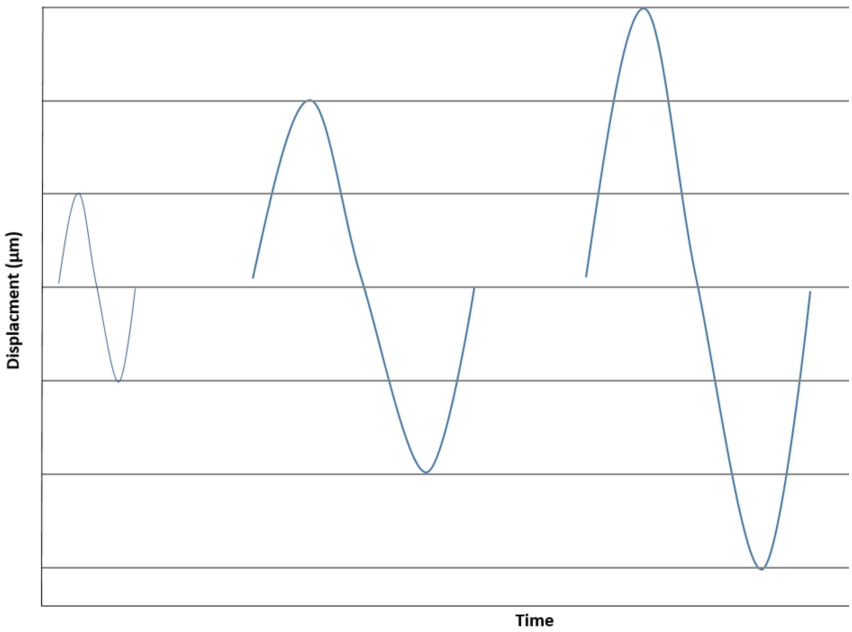

Figure 2.14 Variation of displacement amplitude in an EBADE test

2.4.4.6 Double Edge Notched Tensile (DENT) Test

It is an improved version of the force-ductility test based on the theory of essential work of fracture compared to the empirical force ductility test. It has also been standardized in the form of a provisional standard as AASHTO TP 113-15 [225]. The DENT test is conducted on short term aged and long term aged samples. The test procedure consists of filling the aluminium molds (Figure 2.15) having different ligament lengths (5, 10, and 15 mm) with the binder and conditioning at 15^{o}C for 3 hours, followed by the demolding [225]. The notched samples are subjected to a constant stretching rate of 50 mm/min until the ductile failure. The load and deformation are recorded continuously during the stretching to determine the failure energy. The DENT test yields strain tolerance in the ductile state in terms of crack tip opening displacement (CTOD) in the presence of critical tensile stresses [226]. Asphalt binder gradings are done in terms of CTOD, which is calculated as the ratio of specific essential work and tensile yield stress [227]. The material that can stretch more before sustaining damage represents better fatigue resistant material; hence, CTOD is the fatigue damage indicator. The

double edged notched geometry can better simulate microcracks formed between two aggregates in an asphalt mixture as compared to undamaged or non-notched samples [228].

Some other binder fracture tests include the Superpave direct tension test (DTT) [229,230] asphalt binder cracking device (ABCD) test [231], fracture energy test [232], compact tension test [233], cyclic shear cooling (CSC) failure test [234], acoustic emission (AE) approach test [235] etc.

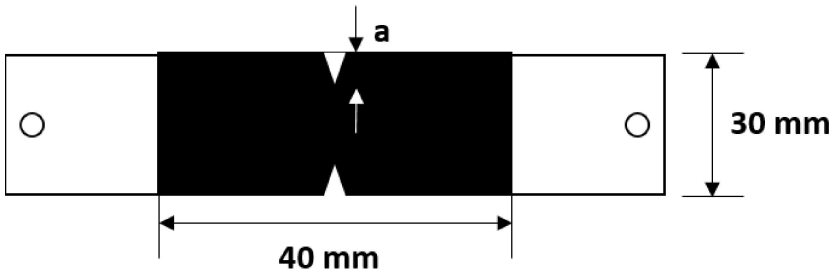

Figure 2.15 Schematic of double edge notched tensile test

2.4.5 Testing Geometry

The fatigue performance of the material is also a primary function of the testing geometry. It decides the response of the material to the applied loading. The shape of the concerned sample determines the distribution of stress in the material and hence affects the fatigue life of the material. Keeping in mind the major contribution of the sample geometry, researchers have experimented with numerous geometries to find the best geometry to evaluate the accurate fatigue characteristics of the material.

2.4.5.1 Cylindrical Geometry

The cylindrical parallel plate geometry is the most common testing geometry used in the DSR for the rheological analysis of asphalt binders [139,236,237] and asphalt mastics [238–241]. It is an 8 mm diameter and 2 mm high specimen geometry generally used for rheological testing at intermediate temperatures, as shown in Figure 2.16. It is used in the majority of studies

across the globe due to its simplicity and easy calculations. The stress and strain in the sample can be calculated based on the applied torque and angular rotation using the following equations from torsional mechanics:

$$\tau = \frac{2T}{\pi r^3} \tag{2.35}$$

$$\gamma = \frac{r.\theta}{h} \tag{2.36}$$

Where τ is the shear stress (N/mm$^{2)}$), γ is the strain, T is the torque (N.mm), r is the radius of the sample (mm), θ is the deflection angle (radians) and h is the plate gap (mm).

Figure 2.16 Elevation view of cylindrical geometry

2.4.5.2 Cone and Plate (CP) Geometry

The uniform stress distribution throughout the sample makes it a better geometry as compared to conventional cylindrical geometry due to the presence of an upper conical plate [41]. The following equations can express the shear stress and shear strain:

$$\tau = \frac{3T}{2\pi r^3} \tag{2.37}$$

$$\gamma = \frac{\theta}{\Phi} \tag{2.38}$$

Where Φ is the cone angle that adjusts the required gap to maintain a uniform strain field Figure 2.17). Motamed and Bahia [242] highlighted that the effect of testing geometry is very dominant on the material properties measured using DSR, especially at higher stress levels and long duration of loading. They showed that the binder might flow out of the standard parallel plate (PP) geometry, called tertiary behavior, in a repeated loading test due to instability resulting in the change in specimen geometry which was not the case with cone and plate geometry.

The plate gap is non-adjustable for the given cone, so the tests can only be conducted at a predetermined height. CP geometry is unsuitable for asphalt mastics as well as CRMB due to the very small gap between the plates, which is not the case with PP geometry.

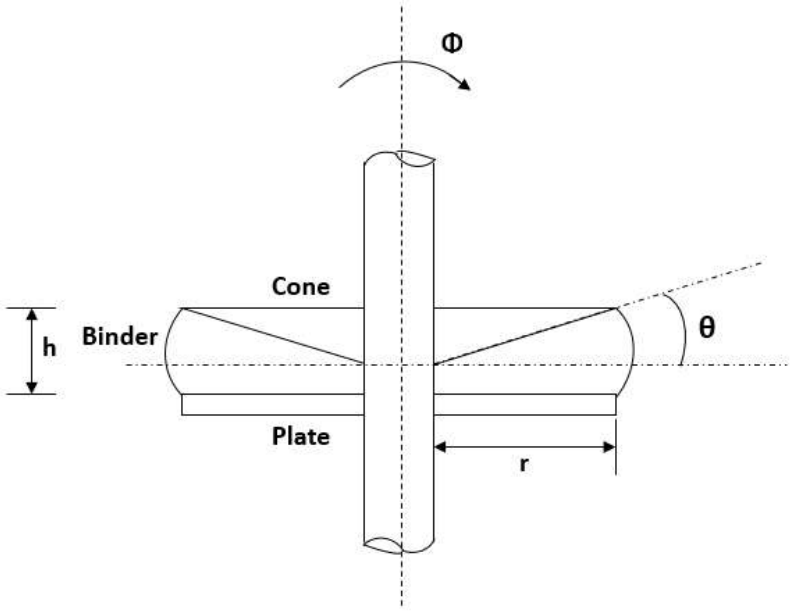

Figure 2.17 Cone and plate geometry [41]

2.4.5.3 Concentric Cylinder (CC) or Bob and Cup Geometry

As the name suggests, it is a bifold cylindrical geometry in which the central cylinder (bob) rotates inside an outer stationary cylinder (cup) to shear the sample between them (Figure 2.18). The surface area of the bob, as well as the inside surface area of the cup, controls the CC geometry. Only the binder between the bob and the cup is considered, whereas the binder above the bob and at the bottom of the cup is ignored [42]. The sample trimming is eliminated in the bob and cup; hence, the errors due to the inaccurate trimming are eliminated. It can accommodate large-sized particles as well, like in CRMB.

The shear stress and shear strain calculations for the CC geometry are shown below:

$$\tau = \frac{T}{2\pi h {R_i}^2} \tag{2.39}$$

$$\gamma = \frac{\theta R_i}{(R_o - R_i)} \tag{2.40}$$

Where T is the torque required, R_o is the radius of the cup, R_i is the radius of the bob, and θ is the angular rotation of the bob.

The sample required is very large compared to the PP test [243]. The longer testing durations (almost twice as with PP geometry) are another drawback associated with bob and cup geometry. The CC geometry is also unsuitable for stiffer materials such as asphalt mastics because the insertion of bub is difficult in stiff mastics [49].

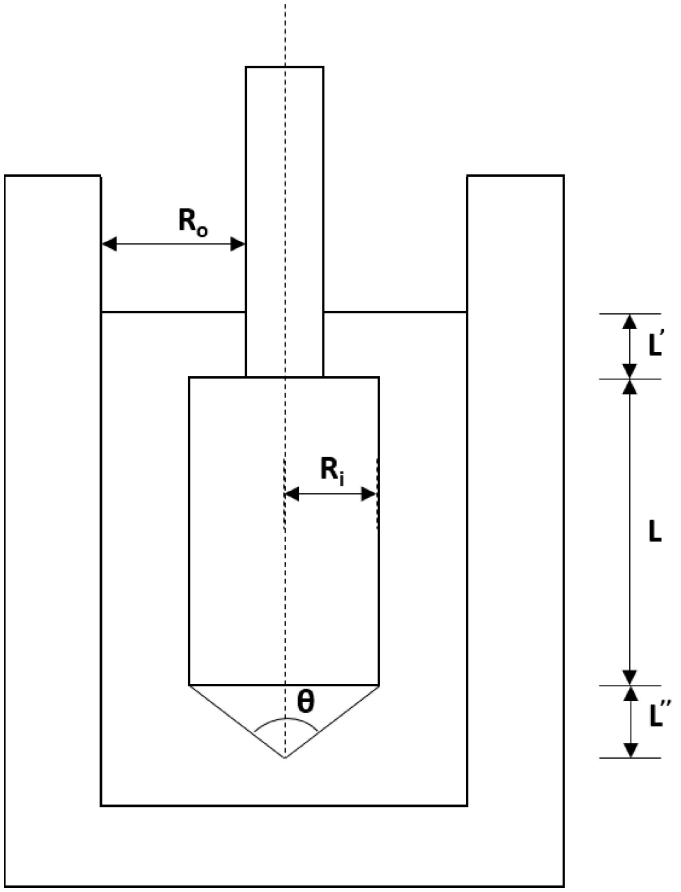

Figure 2.18 Bob and cup geometry [42]

2.4.5.4 Torsion Cylinder (TC) Geometry

Martono et al. [47] investigated the relationship between true fatigue failure and the stiffness of binder by employing the torsion cylinder geometry having 12 mm diameter and 30 mm height along with the PP geometry containing asphalt binder and Ottawa sand (Figure 2.19). The sand-asphalt mixture creates a uniform film thickness to simulate a thin film of the asphalt interface between aggregates in asphalt mixtures. The TC geometry was found to be unaffected by the edge effect because of a significantly higher complex modulus than PP geometry at

different temperatures. In addition to that, TC results were more repeatable and more sensitive to the binder type as compared to its counterpart and hence could be a better geometry to rank the asphalt binders in terms of their fatigue performance.

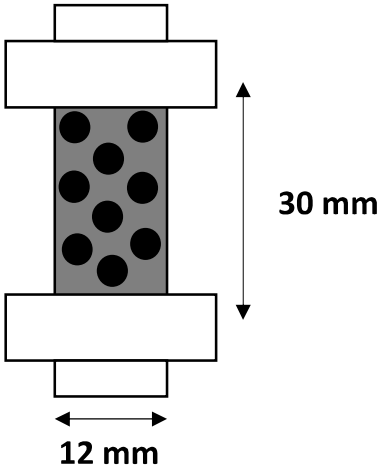

Figure 2.19 Torsion cylinder geometry [47]

2.4.5.5 Vane Geometry

It consists of multiple (generally four) rectangular vanes set at equal angles connected by a central cylinder (Figure 2.20). The advantage of vane geometry lies in the minimal disturbance caused to the asphalt binder due to the insertion of the vane [244]. The vane geometry can be used even to analyze stiffer materials such as asphalt mastics [49]. The primary drawback with vane geometry is that the binder between the vanes may not be sheared, especially at high rotational speeds, which causes inhomogeneous plastic deformation [243]. Hesami et al. [49] recommended 20% filler concentration as a transition point to shift from CC geometry to vane geometry to test asphalt mastics.

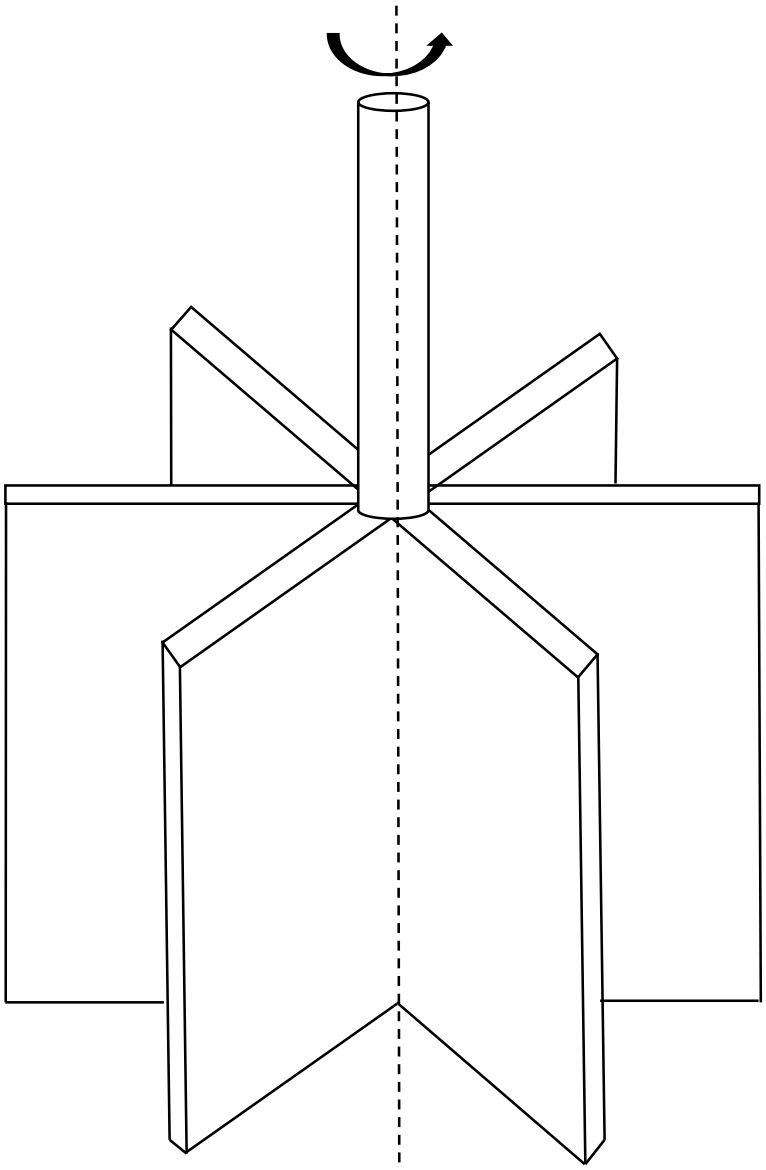

Figure 2.20 Schematic of vane Geometry [49]

2.4.5.6 Parallel Hollow Plate (PHP) Geometry

Apostolidis et al. [46] developed a new testing geometry, the modified version of PP geometry known as a parallel hollow plate (PHP). The PHP testing geometry has a similar outer diameter of 25 mm like conventional geometry and a concentric hollow area of 19 mm diameter and 0.1 mm depth filled with silicon paper before testing. It localized the shear stresses in the periphery

of the sample and hence isolated the damaged area of the binder, as shown in Figure 2.21. This allowed the more realistic prediction of fatigue life compared to PP geometry which overestimates the number of cycles to failure.

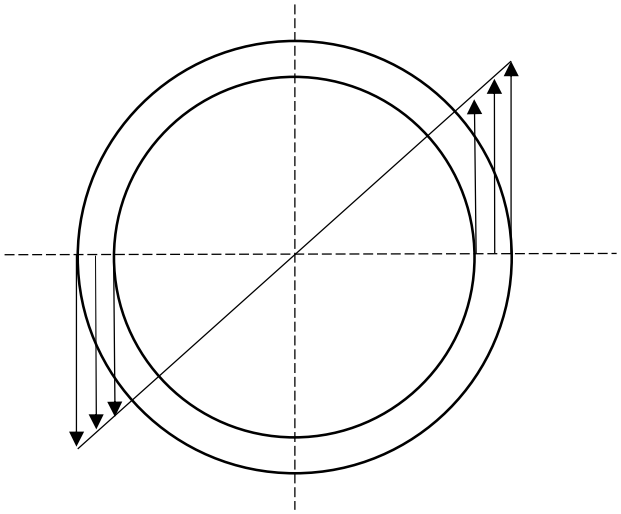

Figure 2.21 Shear stress distribution in PHP geometry [46]

2.4.5.7 Hyperbolic Geometry

Hyperbolic geometry is the modified version of cylindrical geometry with a sample height of 3 mm and a predetermined point of failure at the center of the specimen. The circular necking extending from the ends to the center allows the gradual decrease in the diameter from 8 mm to 6 mm (Figure 2.22). The unfavorable stress concentrations at both ends were minimized by raising a small platform of 0.3 mm at both ends. One of the most important advantages of using hyperbolic geometry is that it can be fabricated in the conventional PP setup, which comes with every DSR. It does not require a separate setup as in the case of a torsion cylinder or vane shear geometry. Unlike other geometries like the Torsion cylinder and vane shear, there is no need to change the setup in the DSR.

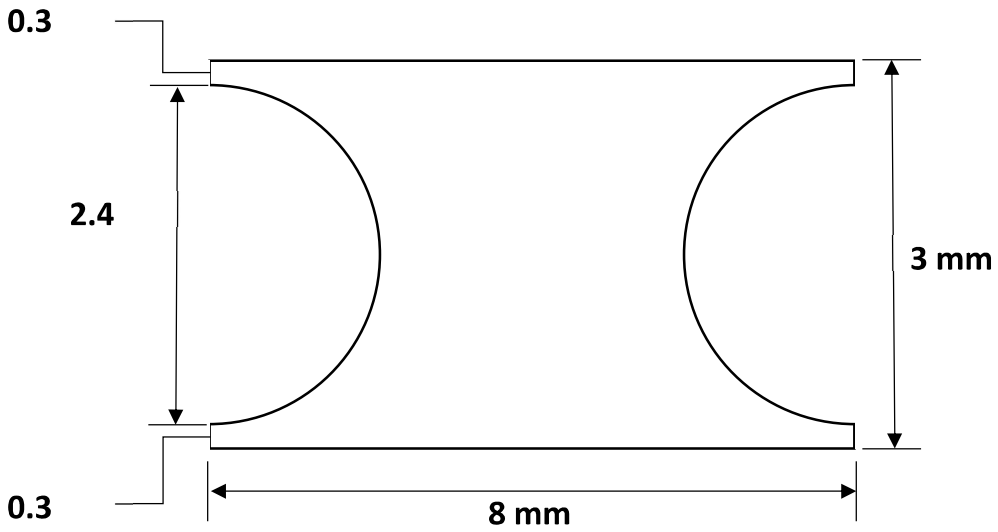

(a)

(b)

Figure 2.22 (a) Elevation view and (b) working test in hyperbolic geometry

2.5 Problem Statement

- The fillers are obtained from the earth's crust by the exhaustive mining of reserves which led to the imbalance in the ecosystem. Due to the immense mining pressure on the crust, authorities have imposed strong restrictions, making access to natural fillers very challenging. As a result, the need for waste derived fillers is high in demand for sustainable construction, which can also be an affordable and environmentally friendly alternative.
- The actual point of failure in the asphalt binder/mastic is not evident during the fatigue testing owing to which the failure point is assumed corresponding to various failure criterias. Therefore, an accurate fatigue testing protocol with precise failure criteria can provide a better damage assessment in the asphalt mastics.
- Also, the rheological analysis, including fatigue testing, is a primary function of the geometry used in the DSR. The resistance of the material against fatigue distress is the intrinsic property of the material and should be independent of the testing geometry. But different geometries yield divergent fatigue properties, due to which the search for a geometry that can accurately characterize the fatigue behavior of asphalt materials is still a long hunt.
- Moreover, The SHRP guidelines have recommended the filler-binder ratio in the range of 0.6 – 1.2 by weight for the satisfactory performance of asphalt pavements which is quite empirical. The waste fillers' characteristics vary widely in terms of gradation, particle shape, surface area, mineralogical composition, and physicochemical properties. Due to this, imposing the same range of filler-binder ratio to every filler may not be judicial, keeping in mind the significant effect of fillers on the performance of asphalt mixes as elucidated by a plethora of research. Therefore, the optimum range of filler contents needs to be readdressed.